# Chapter 1
# Cu@Pt/C Catalysts: Synthesis, Structure, Activity in Oxygen Reduction Reaction

**Anastasia A. Alekseenko, Sergey V. Belenov, Vadim A. Volochaev, Ivan N. Novomlinskiy and Vladimir E. Guterman**

**Abstract** Nanostructured Cu@Pt$_x$/C catalysts with low platinum content ($x = 0.8$), comprising nanoparticles of core-shell architecture, were obtained by method of synthesis, which combines galvanic substitution of Cu at Pt and chemical reduction of Pt(IV). The obtained catalysts show high values of the electrochemically active surface area of platinum 80–100 m$^2$/g (Pt) and higher both activity in the oxygen electroreduction reaction (ORR) and stability compared with commercial Pt/C catalyst HiSPEC 3000 (Johnson Matthey).

## 1.1 Introduction

An actual problem of modern electrochemical power engineering is a preparation of electrocatalysts for low temperature fuel cells, which have desired characteristics for modern technologies [1, 2]. Looking for the ways to optimize of well-known synthesis methods is one of the most promising directions in the field of preparation and study of these materials [2, 3]. It is important reduce a cost of platinum catalysts, for example, by optimizing their composition, by enhancement of activity and stability, and by reducing the total cost of production.

The composition, size, shape and fine structure (architecture) of Pt and Pt-alloys nanoparticles (NPs) are the most important parameters, which affect the basic characteristics of catalysts [4–7]. Preparation of Pt-based electrocatalysts, containing bimetallic NPs with core-shell structure is primarily seen as a good possibility to reduce the loading of expensive platinum in the final material [3, 6]. At the same time, there is a positive influence (promoting effects) of metal core on the catalytic activity of platinum shell in some reactions [3, 6, 8]. As a rule, this effect is often observed in the case of a small thickness of the platinum shell [6, 8].

A.A. Alekseenko (✉) · S.V. Belenov · V.A. Volochaev · I.N. Novomlinskiy · V.E. Guterman
Southern Federal University, Zorge St. 7, 344090 Rostov-on-Don, Russia
e-mail: an-an-alekseenko@yandex.ru

There are various ways of obtaining the electrocatalysts based on core-shell nanoparticles architecture by chemical reduction of precursors. In [6, 9, 10], the authors used a consistent chemical reduction of Pt(IV) on the pre-formed nuclei of $d$-metal (Cu, Ni, Ag, Pd, Co). By using these methods, bimetallic nanoparticles with thick (multilayer) Pt-shell are usually formed [6, 9]. In these NPs would be difficult to expect the promoting effect of the core on the catalytic activity of Pt-shell, and the mass fraction of precious metal in the catalyst is sufficiently high. In addition, the implementation of chemical reduction has difficulties to control the nanoparticles growth process and as usual rather thick Pt-shell is formed [6, 9, 10].

In order to produce NPs with core-shell structure the authors suggest the galvanic replacement method, it has been mentioned in a number of publications [11–17]. When non-noble metal nanoparticles $M_1$ ($M_1$ = Cu, Ag, Au, Pd, Ni, Co) are contacting with noble metal ions ($M_2^{z+}$), the reaction occurs [11–13, 16–18]:

$$M_1 + (n/z)M_2^{z+} \rightarrow M_1^{n+} + (n/z)M_2^0. \tag{1.1}$$
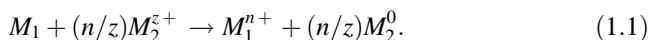
The reaction takes place for the following condition: $E_p$ ($M_2^{z+}/M_2$) $\gg E_p$ ($M_1^{n+}/M_1$), where $E_p$ is the equilibrium potential of the corresponding metal ion [11, 18]. During the electrochemical replacement process, Pt-atoms partially replace atoms $M_1$. By this mechanism 2D [12, 13, 17–19], and 3D-structure [5, 14, 17, 18] may be formed, in time it leads to the formation of a thin Pt-shell (up to a monolayer) on the surface of the $d$-metals. Core-shell nanoparticles with thin Pt layer, are obtained via this method, are often characterized by high activity [5, 13, 17], but the possibility of their long-term functioning as electrocatalyst is questionable due to the low Pt-layer thickness and consequently a low protecting ability of the shell to the metal core. In the most known studies, whose authors describe galvanic replacement method, the replacement of core atoms on platinum atoms is carried out in the sub-micron layers of $d$-metals, the size of these particles is large [11, 15–19]. In addition, a large number of studies [14, 16, 18, 19] describe the synthesis is carried out in an organic medium with stabilizers and without carbon support. Therefore, it is not quite clear what sorts of characteristics will show materials with nanoparticles deposited on the surface of the carbon support.

It should be noted that one of the possible method of improving the characteristics of M@Pt/C catalysts could be a thermo-treatment [20–23]. Evidently, the selected temperature conditions play an important role during this post-treatment [21–23].

In general, the questions about how to obtain the Pt-M nanoparticles with non-uniform distribution of components, suitable for the creation of high-level and relatively stable electrocatalysts, the optimal thickness of the Pt-shell and its control methods of thickness are still relevant.

In the present study, we investigated the possibility of using the combined method of synthesis: the combination of galvanic replacement (GR) of copper on platinum and chemical reduction Pt(IV) to Pt(0) in order to obtain bimetallic NPs with the structure including Cu-core and Pt-shell. In the development of synthesis methods, we proceeded from the assumption that at the first stage (GR) on surface of copper nuclei is formed thin (possibly defective) platinum shell. Pre-deposition

of calculated amount of platinum on the second stage—chemical reduction (ChR) should result in healing of the defects and the formation of a dense shell. Moreover, as noted in the literature review, conducting thermal post-treatment for the synthesized material could lead to higher crystallinity, reduced defectiveness, and consequently enhance the protective ability of Pt-shell relative to the core nanoparticle.

## 1.2 Experimental Part

Initially nanostructured Cu/C material, identified as $A_1$, was obtained by $CuSO_4$ reduction in carbon suspension (Vulcan XC72) by freshly prepared $NaBH_4$ solution. Mass loading of copper (12.5%) in the sample was determined by thermogravimetry. Formed copper nanoparticles were used as cores in further synthesis. The results of powder X-ray diffraction study show the presence of copper phase in combination with small amounts of copper (I) oxide (Fig. 1.1). The calculations according to Scherrer's equation confirmed the presence of the particles (crystallites) of copper with the average size of 10–11 nm.

At the next step, included the galvanic replacement, part of copper was replacing by platinum by adding a portion of $H_2PtCl_6 \cdot 6H_2O$ to Cu/C suspension in ethylene glycol solution:
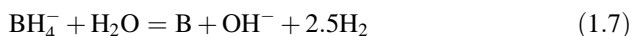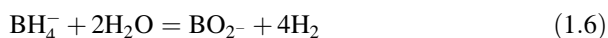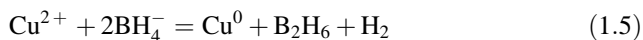
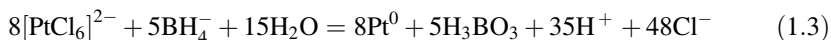$$2Cu^0 + [PtCl_6]^{2-} = Pt + 2Cu^{2+} + 6Cl^-. \tag{1.2}$$
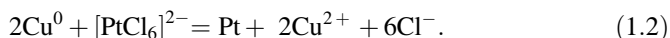
Then a second portion of $H_2PtCl_6 \cdot 6H_2O$ and the excess $NaBH_4$ solution (freshly prepared) were added to reduce Pt(IV) and $Cu^{2+}$ ions, passed into the solution at the previous stage of the synthesis by the reaction (1.2). It is known that
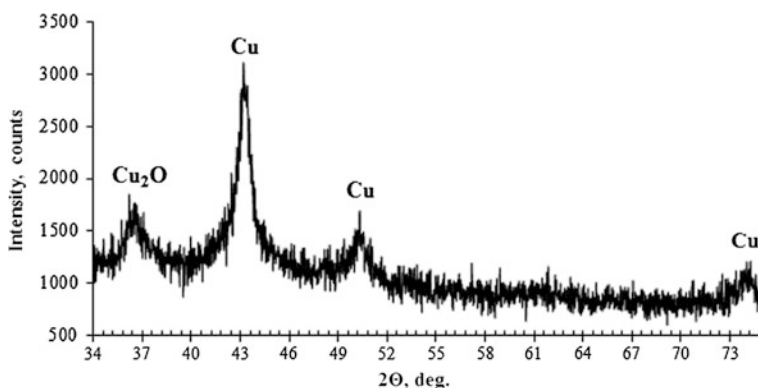


**Fig. 1.1** The XRD-diffractogram of the synthesized Cu/C material ($A_1$)

during the reduction of Pt(IV) and $Cu^{2+}$ by sodium borohydride can proceed the reactions (1.3)–(1.5) [24–26]. Side reaction in the decomposition of sodium borohydride is accompanied by evolution of hydrogen (see, reactions (1.6), (1.7)) can take place simultaneously [25].

$$8[PtCl_6]^{2-} + 5BH_4^- + 15H_2O = 8Pt^0 + 5H_3BO_3 + 35H^+ + 48Cl^- \qquad (1.3)$$

$$[PtCl_6]^{2-} + BH_4^- + 2H_2O = Pt^0 + BO_{2-} + 4H^+ + 6Cl^- + 2H_2 \qquad (1.4)$$

$$Cu^{2+} + 2BH_4^- = Cu^0 + B_2H_6 + H_2 \qquad (1.5)$$

$$BH_4^- + 2H_2O = BO_{2-} + 4H_2 \qquad (1.6)$$

$$BH_4^- + H_2O = B + OH^- + 2.5H_2 \qquad (1.7)$$

The prepared powders of Cu@Pt/C electrocatalyst were separated by filtration of the suspension using a Buchner funnel, washed with acetone and water, and dried in a desiccator over $P_2O_5$ (sample A). Two portions of the resulting sample were chosen for the post-treatment procedure (one hour in an argon atmosphere) at the temperatures of 250 and 350 °C (samples are named as $A_{250}$ and $A_{350}$). Additionally, Cu@Pt/C material was obtained by chemical reduction, as described in [9], and was used as a reference. In this case, the synthesis also was carried out using preformed copper nuclei (Cu/C). Solution of $NaBH_4$ was used as a reducing agent. The prepared Cu@Pt/C electrocatalyst powders were separated by filtration of the suspension using a Buchner funnel, washed with acetone and water, and dried in a desiccator over $P_2O_5$ (sample B).

Synthesis of the samples was repeated according to the described above methods at least three times, that allowed one to evaluate the reproducibility of characteristics for the obtained Cu@Pt/C materials.

The metal content was determined by TG method—the samples were calcined at 800 °C, the value of weight of the material after the calcination was used for calculations, taking in account the oxidation of metal copper to copper oxide (II). Electrochemical behavior of obtained catalysts was compared between the synthesized samples as well as the commercial electrocatalyst HiSPEC3000 (Johnson Matthey, 20% Pt), which was used for the comparison.

In order to determine the ratio of metals in the samples, X-ray fluorescence analysis was used on a Shimadzu EDX-800HS spectrometer at the following conditions: tube voltage—50 kV, current—15–25 mA, acquisition time—100 s. Processing of the X-ray fluorescence spectra was carried out using DXP-700E software (Version 1.00 Rel.017).

ARL X'TRA powder diffractometer with Bragg–Brentano geometry (θ-θ), CuKα—radiation ($\langle \lambda \rangle$ = 0.15418 nm) was used for powder X-ray data collection. Measurements were performed at room temperature. The samples were thoroughly mixed and placed into a cell on a depth of 1.5 mm or on a background-free substrate. Acquisition was carried out in a range of 15–55° with increments of 0.02°

and a rate from 4° to 0.5° per minute, depending on the task. The average size of crystallites was determined by Scherrer's equation for the most intensive peak (111) as described in [27]. Preliminary, the sizes of the crystallites, that are calculated via the FWHM of the (111) reflections for Cu@Pt/C materials are relative, because this peak may actually represent a superposition of the reflections of the two phases on the base of copper and platinum.

Transmission electron microscopy (TEM) analysis was performed using a JEM-2100 microscope operated at an accelerating voltage of 200 kV and resolution of 2 nm. Samples for TEM analysis were prepared by suspending the 0.5 mg catalyst powders in 1 ml of isopropanol. The suspension was ultrasonically dispersed, and one drop of the suspension was deposited onto a copper grid with carbon scattering.

Electrochemical measurements were performed at room temperature in a standard three-electrode cell. The electrolyte was 0.1 M $HClO_4$ solution saturated with Ar at atmospheric pressure. A saturated Ag/AgCl electrode was used as the reference electrode. All potentials cited here are referenced to the standard hydrogen electrode (SHE). The investigated catalyst was applied to the end of the rotating disk electrode in the catalyst's «ink» form, as described in [27].

One hundred cycles of potential sweep were initially recorded in the range from 0.03 to 1.2 V at a speed rate 200 mV/s. Then two CV cycles were registered in the same range of potentials, but upon a speed rate 20 mV/s. The electrochemically active surface area of Pt catalyst (ECSA) was determined by amount of electricity to be used for the electrochemical adsorption/desorption of atomic hydrogen during the registration of the second CV under 20 mV/s. The method of calculation is described in more detailed way in [29].

To evaluate the activity of catalysts in the oxygen reduction reaction (ORR), series of linear sweep voltammograms in a range from 0.020 to 1.2 V were measured (the scan rate 20 mV/s at speeds of disc electrode rotation 400, 900, 1600, 2500 rpm). To compare the activity of the tested catalysts, measured currents were normalized by the mass of platinum (A/g(Pt)).

To assess the stability of the electrocatalyst, a long-time (5000 cycles) voltammetric cycling method has been selected in the three-electrode cell with potential sweep in the range of 0.5–1.0 V with a scan rate of 100 mV/s. After every 500 cycles, two CVs were recorded to calculate ECSA (potential sweep rate of 20 mV/s, the potential range of 0.03–1.2). Stability was evaluated by the value of the degree of degradation (DD, %) by calculating $ECSA_{5000}/ECSA_0$ ratio.

## 1.3   Results and Discussion

The actual composition of obtained metal-carbon materials is close to the composition calculated by precursors loading: the mass fraction of metals—26–28% by weight, the content of Pt—15% by weight (Table 1.1). Thus, the composition of the metal component for each bimetallic material corresponds to the formula $Pt_{0.8}Cu$.

**Table 1.1** Some characteristics of commercial catalyst HiSPEC 3000 and Cu@Pt/C materials prepared by the combined method (A, A250, A350) and chemical reduction (B)

| Sample | Composition of metal component (XRF) | Metal loading (% wt) | | Average size of crystallites, D (nm) | $ECSA_0$ ($m^2$/g (Pt)) | Degree of degradation, DD (%) |
|---|---|---|---|---|---|---|
| | | Estimated | Factual | | | |
| A | $Pt_{0.8}Cu$ | 28.2 | $28 \pm 0.8$ | $2.7 \pm 0.2$ | $100 \pm 10$ | 34 |
| $A_{250}$ | | | | $3.8 \pm 0.3$ | $89 \pm 9$ | 18 |
| $A_{350}$ | | | | $4.5 \pm 0.4$ | $80 \pm 8$ | 33 |
| B | $Pt_{0.8}Cu$ | 30 | $26 \pm 0.8$ | $2.3 \pm 0.2$ | $55 \pm 5$ | 20 |
| HiSPEC 3000 | Pt | – | 20 | $2.2 \pm 0.2$ | $81 \pm 8$ | 33 |

Powder X-ray diffractograms of the obtained materials have a typical for Pt/C and Pt-*M*/C catalysts shape [9, 12, 15]. Wide peaks on diffractograms of Cu@Pt/C samples confirm the presence of nano-sized ptatinum-contained particles (Fig. 1.2). Reducing the broadening of reflections for $A_{250}$ and $A_{350}$ samples (after the heat treatment) is due to the increase in the average crystallite size from 2.7 to 4.5 nm (Fig. 1.2, curves 2, 3; Table 1.1). The offset of platinum reflection (111) in the direction of larger values of $2\Theta$ (the angle range 40–41°) is quite typical for the bimetallic catalysts, and it happens due to the influence of the alloying atoms (copper). Similar effects were observed in the case of formation of disordered solid solutions [12] and during the formation of NPs with Cu-core/Pt-shell architecture [9, 10]. Asymmetry of observed peaks in comparison with Pt/C reflections may be caused by inhomogeneity of phase's distribution (copper and platinum) in NPs. The appearance of small reflections in the area $2\Theta$ nearly 36.2° for thermo-treated samples $A_{250}$ and $A_{350}$ (Fig. 1.2, curves 2 and 4) indicates the presence of copper (I) oxide phase. Apparently, a small amount of amorphous copper (I) oxide originally was contained in the sample A, and its heat treatment resulted to formation of crystal structure $Cu_2O$, visible for powder X-ray method. Even a little quantity of oxygen, contained in the pores of the carbon support, could oxidize the not protected by a continuous platinum shell copper, despite the fact that the heat treatment is conducted in an inert atmosphere.

Catalysts A and B were studied by transmission electron microscopy (TEM). It indicates the presence in their structure of NPs, which differ significantly in size and, possibly, in architecture. The initial copper cores in Cu/C material represent large NPs or their aggregates (Fig. 1.3a–c). So, it is not surprising that large NPs or aggregates of 10–12 nm size are presented in the TEM images of the sample A (Fig. 1.3d–f). We believe that such particles are formed, as a result, of platinum deposition during the synthesis on the surface of previously obtained copper particles. Calculation of interplanar distances, conducted by TEM results for the initial Cu/C material (Fig. 1.3b–c) indicated the presence of two phases—Cu and of $Cu_2O$. In this case, copper (I) oxide surrounds some copper NPs. It is not clear whether the formation of copper oxide (I) happens—directly during synthesis or later on: during filtering, washing, drying and storage of Cu/C samples. Apparently, during the

**Fig. 1.2** XRD-diffractograms of $1$—A, $2$—$A_{250}$, $3$—$A_{350}$, $4$—B
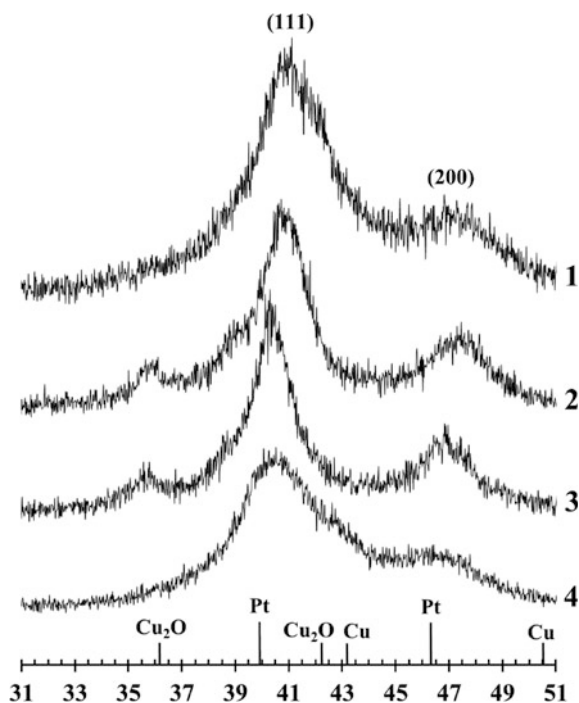
subsequent formation of platinum shell, a significant portion of copper (I) oxide, previously dissolved in an acidic medium, was re-deposited as $Cu^0$ together with platinum. Platinum deposition process is accompanied by the destruction of large portion of copper nanoparticle aggregates. This conclusion can be made by comparing the particle size of Cu@Pt, formed during galvanic replacement, as previously observed in [11]. This fact may explain the smaller particle size after the formation of Pt-shell (Fig. 1.3d–f), compared with the size of initial copper nuclei (Fig. 1.3a–c). Significantly larger size of NPs in according with TEM results, compared with the size of the crystallites by XRD results (Table 1.1), could be caused by both a complex architecture of the NPs and by the presence of the amorphous transition layer on the interface boundary. In addition, individual bimetallic NPs can consist of a number of crystallites.

It is also possible to see large particles or nanoparticle's aggregates of 10–12 nm on TEM images for the sample B, which was prepared by chemical deposition of platinum on the Cu/C. Some NPs are in the size more than 10 nm and possess the expressed core-shell structure (Fig. 1.3g–i). Note that the presence of the contrast between the shell and core in the TEM images is not a precondition for confirmation of this architecture. Usually the contrast is characteristic of the large particles with thick shell [9, 15, 18]. A significant proportion of such Cu@Pt NPs is detected in the sample B. The TEM microphotographs of fragments of surface for
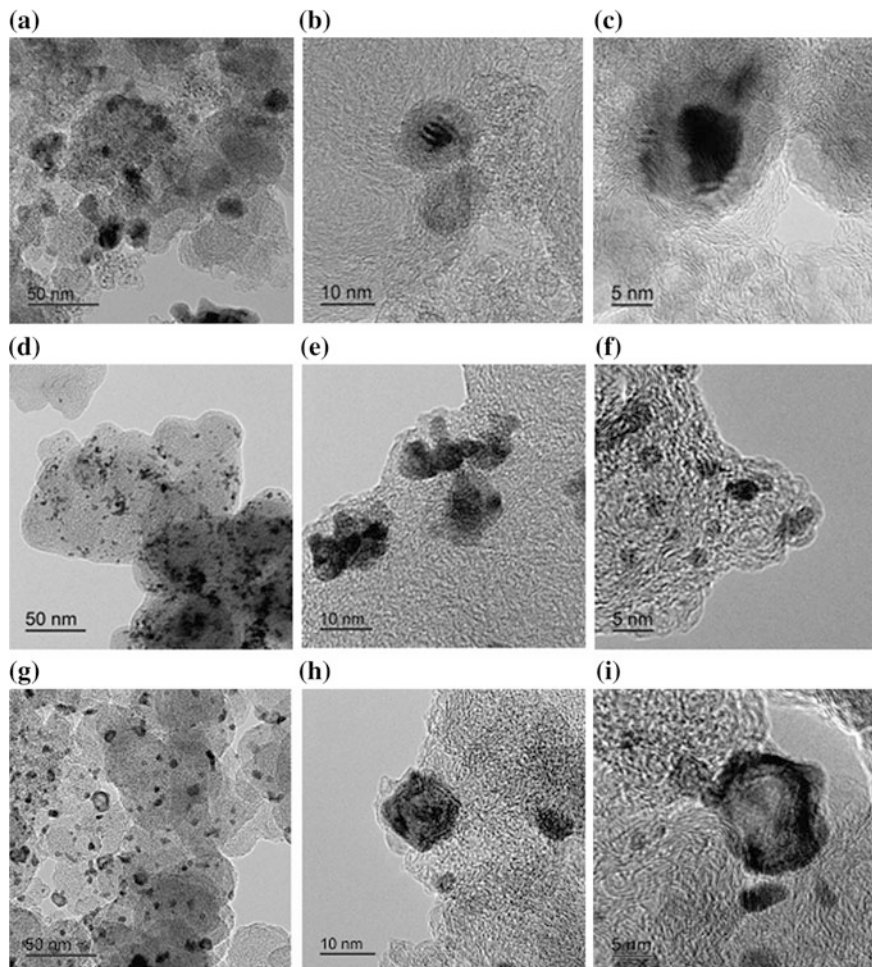
**Fig. 1.3** Transmission electron microscopy photographs of the surface for Cu/C and Cu@Pt/C materials: **a–c** sample Cu/C—$A_1$ (core); **d–f** sample Cu@Pt/C—A (combined synthesis method); **g–i** sample Cu@Pt/C—B (chemical reduction method)

sample A (Fig. 1.3d–f) show NPs for which there is no contrast between the shell and the core. This does not exclude the possibility for them to have a relatively thin platinum shell [12].

In the microphotographs of A and B samples, 2–3 nm NPs can be seen (Fig. 1.3d–i). These NPs may represent a core-shell structure, or the one-phase particles. The latter could be formed by deposition of platinum (co-deposition of platinum and copper) on a carbon support during galvanic replacement step (by electrochemical mechanism, sample A), and at the stage of the chemical reduction (samples A and B). At the same time, it does not exclude the possibility of appearing small size NPs composed of a platinum or solid platinum-copper solution, in catalysts A and B.

A high copper content in the obtained samples A and B was confirmed by X-ray fluorescence analysis (Table 1.1). Moreover, during the pretreatment, Cu@Pt/C samples on the anodic branches CV copper dissolution peaks (Fig. 1.4a) were not recorded (Fig. 1.4b, c). This indicates the absence of direct contact of the electrolyte with copper NPs or copper cores, which poorly protected by the platinum shell.

Sample A demonstrates higher current values in the hydrogen area on CV compared with sample B (Fig. 1.5). Despite the relatively large size of the NPs (Table 1.1) $ECSA_0$-values of these catalysts were respectively 55 and 100 m$^2$/g(Pt).



**Fig. 1.4** The cyclic voltammograms at the stage of standardization: **a** sample Cu/C—A$_1$ (initial cores), **b** sample Cu@Pt/C—A (combined synthesis method), **c** sample Cu@Pt/C—B (chemical reduction method). De-aerated 0.1 MHClO$_4$, room temperature. Scan rate —200 mV/s
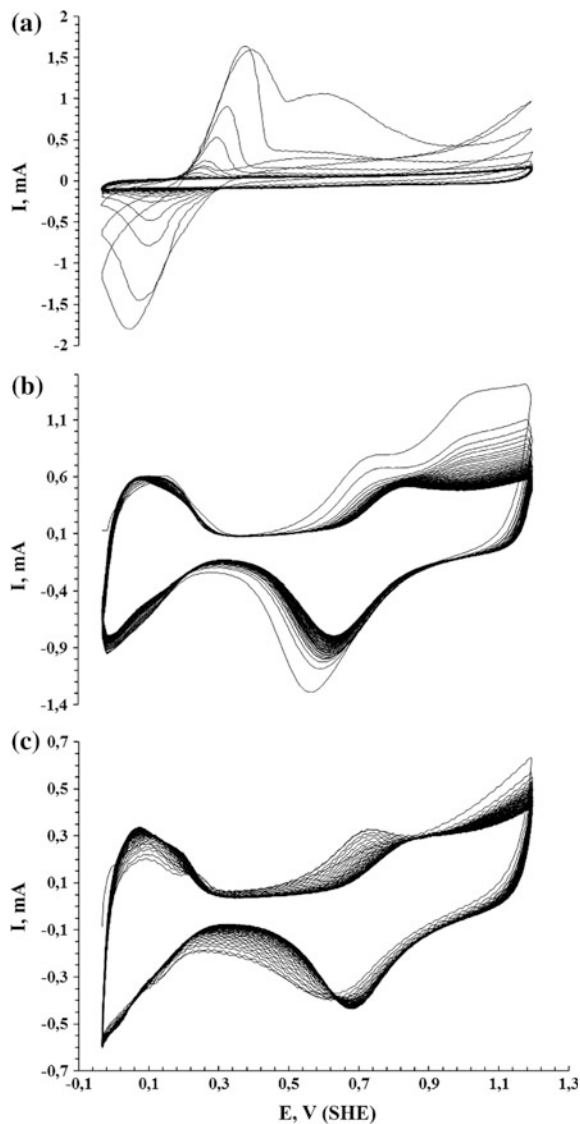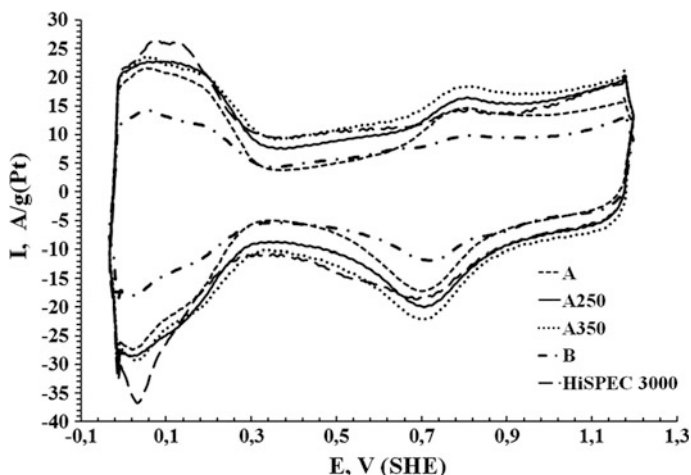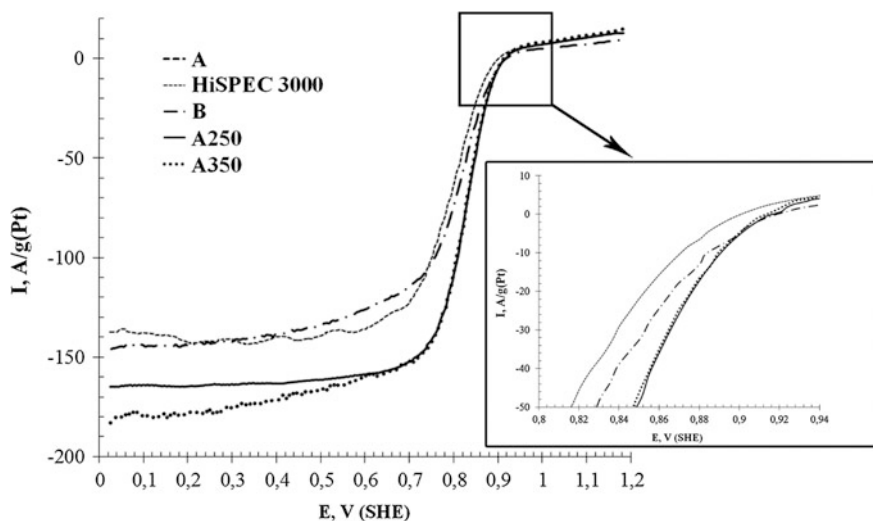
**Fig. 1.5** CV curves of Cu@Pt/C and commercial Pt/C electrocatalysts. Ar-saturated 0.1 M HClO$_4$, room temperature, sweep rate: 20 mV/s

Note that so high value of ECSA$_0$ for materials with medium-sized NPs may be caused by the presence of a significant proportion of particles with the core-shell structure in these catalysts. The fact is that in the case of the material with core-shell structure of NPs, S is determined not so much by their size, but mostly by the thickness of the shell.

For the thermo-treated samples A$_{250}$ and A$_{350}$ was found a ECSA$_0$ reduction effect from 100 to 80 and 89 m$^2$/g(Pt) respectively compared to the initial material A (Table 1.1). This effect may be associated with an increase in the average crystallite size (Fig. 1.5; Table 1.1), due to coalescence of the smallest of them with one another or with larger NPs. In addition, copper oxide formation (Fig. 1.2, curves 2 and 3) can result in lower value of S. The comparison of voltammograms for the samples A, A$_{250}$ and A$_{350}$ (Fig. 1.5) shows that the decrease of ECSA$_0$ for the thermo-treated samples does not lead to lower currents in the hydrogen CV area but increases the current in double-layer region. This effect may be associated with the changing composition of functional groups and the development of the carbon support surface [21]. However, even after the thermo-treatment, the values of S$_0$ for series A samples remain high enough—about the same as the commercial catalyst HiSPEC 3000, and significantly higher than S$_0$ for sample B.

Thermal post-treatment increases the mass activity of Cu@Pt/C electrocatalysts in ORR: for A$_{250}$ and A$_{350}$ samples ORR begins at higher potentials (Fig. 1.6). Current values in the diffusion-kinetic region of the polarization curve (0.7–0.9 V) are higher than values of current for catalysts A, HiSPEC 3000 and B (Fig. 1.6).

As a result of the stress test obtained Cu@Pt/C electrocatalysts showed high stability, not inferior to (A, A$_{350}$) or exceeding (B, A$_{250}$) stability of the commercial

**Fig. 1.6** LSV curves of Cu@Pt/C and commercial Pt/C electrocatalysts. $O_2$-saturated 0.1 M HClO$_4$, room temperature, sweep rate: 20 mV/s, rotation speed: 1600 rpm
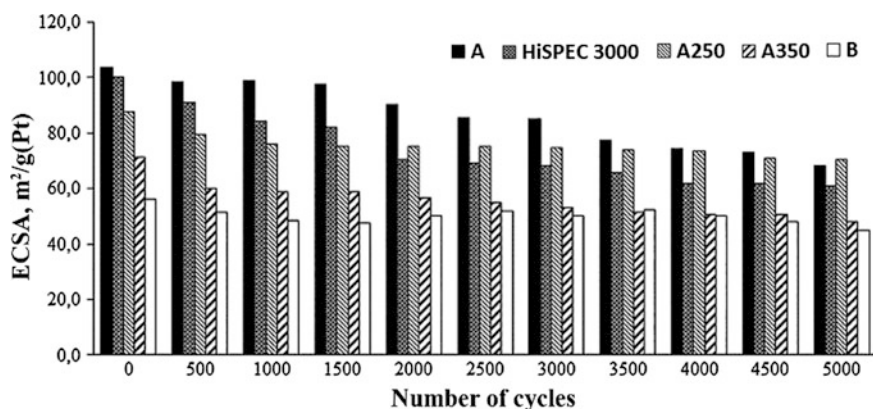


**Fig. 1.7** Dependence of the ECSA on the number of cycles for Cu@Pt/C and commercial Pt/C samples

catalyst HiSPEC 3000 (Table 1.1). The absolute values of S and the nature of their changes over 5000 cycles (Fig. 1.7) are important along with the value of the degradation degree of the active surface of the catalyst after completion of the stress test (Table 1.1).

The highest values of ECSA in the process of testing retained sample A, which was obtained by the combined method—GR + ChR (Fig. 1.7). It is known that the stability of Pt/C electrocatalysts is the greater, the higher average size of the NPs,

bigger mass fraction of Pt in the catalyst and lower $ECSA_0$ value other conditions being equal [9, 29]. Sample B, characterized by the lowest value $ECSA_0$, and, unexpectedly, the sample $A_{250}$, which retained fairly high absolute values of ECSA in the testing process (Fig. 1.7), have been the most stable among studied materials. A similar effect of improving the behavior of the electrocatalyst after thermo-treatment, apparently associated with the ordering of the structure for the core-shell Co@Pt nanoparticles, was observed in [20, 21, 23]. A further increase of temperature during post-treatment of Cu@Pt/C catalyst to 350 °C led to reduction of its stability (samle $A_{350}$) (Table 1.1; Fig. 1.7). Therefore, thermo-treatment of Cu@Pt/C catalysts can lead to increased catalyst activity and stability, however, for each material is necessary to select the optimum treatment temperature and duration.

Thus, a sample $A_{250}$, obtained by the combined method and thermo-treated at 250 °C, has shown the best mass-activity and stability among studied materials. Combined synthesis methods of materials described in this study is perspective for obtaining high-active cathode catalysts for use in low temperature fuel cells.

## 1.4  Conclusions

Cu@$Pt_{0.8}$/C electrocatalysts, containing NPs of core-shell structure and characterized by low (about 15 wt%) content of Pt, have been prepared by chemical reduction of $Cu^{2+}$ and Pt(IV) (sample B), as well as by combining galvanic replacement of copper on platinum and chemical reduction of Pt(IV) (sample A). The electrochemically active surface area of the platinum in A electrocatalyst was about 100 $m^2$/g(Pt). This is significantly higher than that in the commercial Pt/C electrocatalyst HiSPEC 3000 (81 $m^2$/g(Pt)).

Catalysts $A_{250}$ and $A_{350}$, obtained by thermo-treatment of Cu@$Pt_{0.8}$/C (sample A), showed improved ORR activity in comparison with HiSPEC 3000 and «as-prepared» Cu@$Pt_{0.8}$/C materials (A and B). The increased stability during long cycling is a remarkable characteristic of $A_{250}$ and B samples in comparison with other studied catalysts (HiSPEC 3000, A, $A_{350}$). Apparently, the thermo-treatment at 250 °C improves strength characteristics of the platinum shell, without leading to disruption of the complex architecture of bimetallic nanoparticles.

Optimization methods for the synthesis of electrocatalysts, containing Pt-M NPs with core-shell architecture, have a considerable interest. The combined synthesis method that includes galvanic replacement and chemical reduction is a promising tool for Cu@Pt/C catalysts development. This method is characterized by low content of Pt, high values of $S_0$, good activity in the ORR and corrosion-morphological stability.

The results of this research indicate that electrocatalysts containing bimetallic NPs with shell-core architecture are promising objects for testing in low-temperature hydrogen-air fuel cell.

# References

1. A.B. Yaroslavtsev, Y.A. Dobrovolsky, N.S. Shaglaeva, L.A. Frolova, E.V. Gerasimova, E.A. Sanginov, Russ. Chem. Rev. **81**, 191 (2012)
2. D. Thompsett, Catalysts for the proton exchange membrane fuel cell, in *Handbook of Fuel Cells. Fundamentals, Technology and Applications*, vol. 3, p. 1 (2003)
3. H. Yang, Angew. Chem. Int. Ed. **50**, 2674 (2011)
4. Q. Lv, J. Chang, W. Xing, Ch. Liu, RSC Adv. **4**, 32997 (2014)
5. C. Xu, Y. Liu, J. Wang, H. Geng, H. Qiu, ACS Appl. Mater. Interfaces **3**, 4626 (2011)
6. M. Oezaslan, F. Hasche, P. Strasser, J. Phys. Chem. Lett. **4**, 3273 (2013)
7. L. Ou, Comput. Theor. Chem. **1047**, 69 (2014)
8. R.N. Singh, R. Awasthi, C.S. Sharma, Int. J. Electrochem. Sci. **9**, 5607 (2014)
9. V.E. Guterman, S.V. Belenov, A.Y. Pakharev, M. Min, N.Y. Tabachkova, E.B. Mikheykina, L.L. Vysochina, T.A. Lastovina, Int. J. Hydrogen Energy **41**, 1609 (2016)
10. H. Zhu, X. Li, F. Wang, Int. J. Hydrogen Energy **36**, 9151 (2011)
11. B.I. Podlovchenkoz, T.D. Gladysheva, A.Y. Filatov, L.V. Yashina, Russ. J. Electrochem. **46**, 1272 (2010)
12. J. Georgieva, E. Valova, I. Mintsouli, S. Sotiropoulos, S. Armyanov, A. Kakaroglou, A. Hubin, O. MiSteenhaut, J. Dille, J. Appl. Electrochem. **44**, 215 (2014)
13. A. Sarkar, A. Manthiram, J. Phys. Chem. C **114**, 4725 (2010)
14. M. Ji, Y. Zhang, J. Liu, J. Zhang, H. Zhu, Nano Res. **8**, 271 (2015)
15. M. Mohl, D. Dobo, A. Kukovecz, Z. Konya, K. Kordas, J. Wei, R. Vajtai, P.M. Ajayan, J. Phys. Chem. C **115**, 9403 (2011)
16. E. Sutter, K. Jungjohann, S. Bliznakov, A. Courty, E. Maisonhaute, S. Tenney, P. Sutter, Nat. Commun. **5**, 4946 (2014)
17. Z. Li, Ch. He, V. Cai, Sh Kang, P.K. Shen, Int. J. Hydrogen Energy **37**, 14152 (2012)
18. X. Xia, Y. Wang, A. Ruditskiy, Y. Xia, Adv. Mater. **25**, 6313 (2013)
19. M. Tsuji, M. Hamasaki, A. Yajima, M. Hattori, T. Tsuji, H. Kawazum, Mater. Lett. **121**, 113 (2014)
20. R. Lin, T. Zhao, M. Shang, J. Wang, W. Tang, V. Guterman, J. Ma, J. Power Sources **293**, 274 (2015)
21. C.W.B. Bezerra, L. Zhang, H. Liu, K. Lee, A.L.B. Marques, E.P. Marques, H. Wang, J. Zhang, J. Power Sources **173**, 891 (2007)
22. V.E. Guterman, S.V. Belenov, V.V. Krikov, L.L. Vysochina, W. Yohannes, N.Y. Tabachkova, E.N. Balakshina, J. Phys. Chem. C **118**, 23835 (2014)
23. A.N. Valisi, T. Maiyalagan, L. Khotseng, V. Linkov, S. Pasupathi, Electrocatalysis **3**, 108 (2012)
24. H.H. Ingelsten, R. Bagwe, A. Palmqvist, M. Skoglundh, Ch. Svanberg, K. Holmberg, D.O. Shah, J. Colloid Interface Sci. **241**, 104 (2001)
25. J. Qing-lai, P. Zhong-dong, X. Xiao-feng, D. Ke, H. Guo-rong, L. Ye-xiang, Trans. Nonferrous Met. Soc. China **21**, 127 (2011)

26. R.A. Soomro, S.T.H. Sherazi, N.M. Sirajuddin, M.R. Shah, N.H. Kalwar, K.R. Hallam, A. Shah, Adv. Mater. Lett. **4**, 191 (2014)
27. S.A. Kirakosyan, A.A. Alekseenko, V.E. Guterman, V.A. Volochaev, N.Y. Tabachkova, Nanotechnol. Russ. **11**, 287 (2016)
28. V.E. Guterman, A.Y. Pakharev, N.Y. Tabachkova, Appl. Catal. A **453**, 113 (2013)
29. V.E. Guterman, T.A. Lastovina, S.V. Belenov, N.Y. Tabachkova, V.G. Vlasenko, I.I. Khodos, E.N. Balakshina, J. Solid State Electrochem. **18**, 1307 (2014)